Progress In Electromagnetics Research, Vol. 114, 159–175, 2011

A GEOMETRIC METHOD FOR COMPUTING THE NODAL DISTANCE DISTRIBUTION IN MOBILE NETWORKS

K. B. Baltzis

RadioCommunications Laboratory
Section of Applied and Environmental Physics
Department of Physics
Aristotle University of Thessaloniki, Greece

Abstract—This paper presents a geometrically based method for the calculation of the node-to-node distance distribution function in circular-shaped networks. In our approach, this function is obtained from the intersection volume of a sphere and an ellipsoid. The method is valid for both overlapping and non-overlapping networks. Simulation results and comparisons with methods in the literature demonstrate the efficacy of the approach. The relation between networks geometric parameters and distance statistics is explored. As an application example, we model distance-dependent path loss and investigate the impact of channel characteristics and networks size on signal absorption. The aforementioned model is a useful and low-complexity tool for system-level modeling and simulation of mobile communication systems.

1. INTRODUCTION

An important characteristic of mobile networks is the random distribution of the distance between pairs of communicating nodes. Distance statistics are strictly related to system parameters and performance metrics such as capacity, connectivity, link reliability, error probability, hop distance, interference, path loss, etc. In fact, knowledge of the node-to-node (nodal) distance distribution is essential for system configuration, throughput analysis and protocol design [1–4].

Calculation of distance statistics requires information about networks topology and node spatial distribution. Among various

Received 21 December 2010, Accepted 9 February 2011, Scheduled 24 February 2011
Corresponding author: Konstantinos B. Baltzis (kbaltzis@auth.gr).

approaches, methods that assume circular-shaped networks and/or uniform node distribution are popular in mobile networking, e.g., [1, 2, 5, 6]. The authors in [1], established the mathematical framework for the distance distribution between a single point and a round shaped-layer yielding analytical expressions for the outage probability and block error rate in spread spectrum systems. In [2], the distance density between two users uniformly distributed within a circular disk was expressed in closed-form and applied in the analysis of spectral efficiency in decentralised wireless networks. An accurate but cumbersome expression for computing the distance density between points in two circles was derived in [5]. In [6], the application of polynomial regression techniques [7] led to simple expressions that adequately describe the distance density between nodes in non-overlapping circular-shaped networks.

In our analysis, we develop a geometrical-based method [8–15] and provide simple integral expressions for the cumulative distribution function (cdf) of the distance between nodes that are uniformly located within circular-shaped networks. To the best of the author's knowledge, computation of distance distribution includes awkward expressions and requires time-consuming calculations [5]. In the proposed model, the desired cdf is easily obtained from the intersecting volume of a sphere and an ellipsoid with dimensions defined from networks size. Comparisons with simulation results and methods in the literature validate the method. The study of the impact of separation distance and networks radii on distance cdf provides interesting results.

Knowledge of the distance cumulative distribution function allows the calculation of network characteristics such as network capacity, cochannel interference, transmission quality and reliability of communication paths [16, 17]. In this paper, we use the aforementioned model and derive the distance-dependent path loss cdf. A discussion on the relation between channel parameters, networks size and signal absorption demonstrates the efficacy of the approach.

The rest of the paper is organized as follows: Section 2 describes the system model and assumptions and Section 3 presents the proposed model. Comparisons with simulation results and methods in the literature are performed in Section 4. In Section 5, we investigate the impact of system geometry on distance cdf and discuss an application in path loss modeling. Finally, Section 6 concludes the paper.

2. SYSTEM MODEL AND ASSUMPTIONS

We consider two circular-shaped networks with radii $R_{1,2}$ and centers located at distance D from each other (within this context, we will

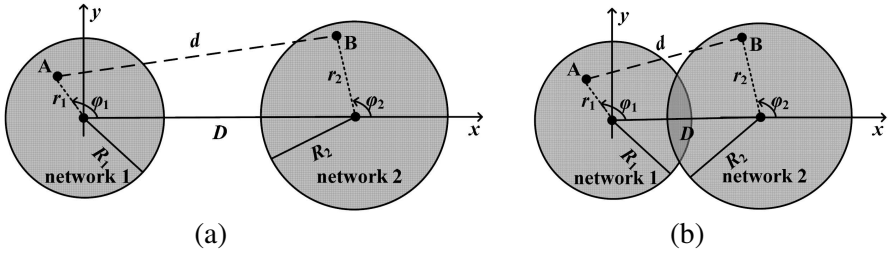

Figure 1. System geometry: (a) non-overlapping and (b) overlapping networks.

call it separation distance), see Fig. 1. The condition $D < R_1 + R_2$ determines whether the networks intersect or not. The system is equivalent to a single network when $D = 0$ and $R_1 = R_2$.

Now, let us consider the nodes A and B with Cartesian coordinates $(r_1 \cos\phi_1, r_1 \sin\phi_1)$ and $(D + r_2 \cos\phi_2, r_2 \sin\phi_2)$, respectively, where $r_{1,2} \in [0, R_{1,2}]$ and $\phi_{1,2} \in [0, 2\pi]$. Under the assumption of uniform node distribution, $r_{1,2}$ and $\phi_{1,2}$ are random variables with densities

$$f_{r_{1,2}}(r_{1,2}) = \begin{cases} \frac{2r_{1,2}}{R_{1,2}^2}, & 0 \le r_{1,2} \le R_{1,2} \\ 0, & \text{otherwise} \end{cases} \qquad (1)$$

$$f_{\phi_{1,2}}(\phi_{1,2}) = U(0, 2\pi)$$

Notation $U(x_1, x_2)$ denotes the uniform distribution in the range $[x_1, x_2]$. In this system, the node-to-node distance is the random variable

$$d = \sqrt{(r_1 \cos\phi_1 - (D + r_2 \cos\phi_2))^2 + (r_1 \sin\phi_1 - r_2 \sin\phi_2)^2} \qquad (2)$$

3. THE NODAL DISTANCE DISTRIBUTION MODEL

In this Section, we compute the distance distribution between nodes that are uniformly distributed within two circular-shaped networks. A special case of this problem was studied in [1]. In that work, the cdf of the distance between a circular disk and a single point was obtained from the intersection area of two circles with radii the disk radius and the link distance.

The proposed model calculates distance cdf as a function of three independent variables, the networks radii and the separation distance. Therefore, the cdf may be obtained from the intersection volume of two solids; see, for example, [18–20].

In 3D space, the circle with radius the link distance (see [1]) is generalized to a sphere with same radius. Similarly, the generalization of the circular disk with radius the network radius (see [1]) is a solid with dimensions determined from the networks radii. The networks radii are two of the independent variables in the problem. Obviously, our scenario is similar to the one discussed in [1] for $R_2 \to 0$ ($R_1 \to 0$) and disk radius equal to R_1 (R_2). Based on the above observations, we set two of the semi-axes of the solid equal to R_1 and R_2. Our study has shown that an ellipsoid with these semi-axes is a proper choice for our model because it further allows the calculation of distance cdf with adequate accuracy without increasing the complexity of the formulation. The third semi-axis of the ellipsoid is related to the others and it is set empirically (further discussion follows below). Finally, we locate the centers of the sphere and the ellipsoid at distance D [19] (recall that in [1], the centers of the two circles were placed at distance equal to the distance between the single point and the network's center).

On the basis of the aforementioned analysis, we approximate the desired cdf as the ratio between the intersection volume of an ellipsoid with position and size determined from system geometry and a sphere centered at the coordinates origin and radius the link distance to the volume of the ellipsoid (in [1], the distance cdf was obtained from the ratio of the overlapping area of two circles with radii the link distance and the network's radius to the area of the second circle).

Let us now consider an ellipsoid with semi-axes a, b and c and a sphere with radius R. The solids are centered at $(x_0, 0, 0)$ with $x_0 \geq a$ and at $(0, 0, 0)$, respectively, see Fig. 2. In spherical coordinates, their surfaces are described by

$$\left(\frac{\cos^2\phi\sin^2\theta}{a^2}+\frac{\sin^2\phi\sin^2\theta}{b^2}+\frac{\cos^2\theta}{c^2}\right)r_e^2-\frac{2x_0\cos\phi\sin\theta}{a^2}r_e+\left(\frac{x_0}{a}\right)^2 -1=0 \tag{3}$$

$$r_c - R = 0 \tag{4}$$

For arbitrary $\phi \in [-\pi, \pi]$ and $\theta \in [0, \pi]$ Equation (3) has two complex solutions,

$$r_{e\pm} = \frac{1}{b^2c^2\cos^2\phi\sin^2\theta + a^2c^2\sin^2\phi\sin^2\theta + a^2b^2\cos^2\theta} \left(x_0b^2c^2\cos\phi\sin\theta \pm abc\sqrt{b^2c^2\cos^2\phi\sin^2\theta-\left(x_0^2-a^2\right)\left(c^2\sin^2\phi\sin^2\theta+b^2\cos^2\theta\right)}\right) \tag{5}$$

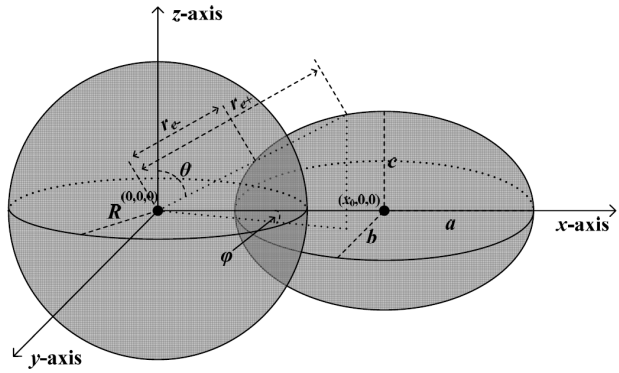

Figure 2. Model geometry.

Obviously, $r_{e\pm} \in \mathbf{R}^+$ that imposes on ϕ and θ the constraints:

$$\begin{aligned} &x_0 bc\cos\phi\sin\theta \\ \geq &a\sqrt{b^2c^2\cos^2\phi\sin^2\theta - \left(x_0^2 - a^2\right)\left(c^2\sin^2\phi\sin^2\theta + b^2\cos^2\theta\right)} \\ &b^2c^2\cos^2\phi\sin^2\theta \geq \left(x_0^2 - a^2\right)\left(c^2\sin^2\phi\sin^2\theta + b^2\cos^2\theta\right) \end{aligned} \quad (6)$$

In order to obtain the desired cdf, we first calculate the intersection volume V between the sphere and the ellipsoid. In our analysis, we compute V from the sum of the volumes of infinite number of elementary pyramidal frustums. Each of these frustums is obtained from the intersection of a semi-infinite pyramid defined from the four rays that emanate from the coordinates origin at directions pointing at angles (ϕ, θ), $(\phi + \Delta\phi, \theta)$, $(\phi, \theta + \Delta\theta)$ and $(\phi + \Delta\phi, \theta + \Delta\theta)$ with $\Delta\phi \ll \phi$ and $\Delta\theta \ll \theta$ with i) the ellipsoid at $r = r_{e-}$ and ii) the ellipsoid (sphere) at $r = r_{e+}$ ($r = R$) when $r_{e+} < R$ ($r_{e+} \geq R$). The top and bottom areas and the height of each frustum are $r_{e-}^2 \Delta\theta\Delta\phi$, $\left(\min\left(r_{e+}, R\right)\right)^2 \Delta\theta\Delta\phi$ and $\min\left(r_{e+}, R\right) - r_{e-}$, respectively.

The volume of a pyramidal frustum with height h and top and bottom areas $A_{1,2}$ is $h\left(A_1 + A_2 + \sqrt{A_1 A_2}\right)/3$ [21]. Considering also the constraints imposed by (6) and the symmetry of the model with respect to the $z = 0$ and $y = 0$ planes, we find that

$$V = \frac{4}{3}\int_0^{\Phi}\int_{\Theta}^{\pi/2}\left(\left(\min\left(r_{e+}, R\right)\right)^3 - r_{e-}^3\right)\sin\theta d\theta d\phi, \ \forall\theta \in [\Theta, \pi/2] : r_{e\pm} \in \mathbf{R}^+ \quad (7)$$

with

$$\Phi = \tan^{-1}\left(b\Big/\sqrt{x_0^2 - a^2}\right) \text{ and } \Theta = \cot^{-1}\left(c\Big/\sqrt{x_0^2 - a^2}\right), \quad (8)$$

the solutions of $r_{e+} = r_{e-}$ at $\theta = \pi/2$ and $\phi = 0$, respectively.

As a result, the desired cdf $F_d(d)$ is approximately (recall that the volume of the ellipsoid is $4\pi abc/3$) equal to

$$F_d(d) \approx \frac{1}{\pi abc} \int_0^{\Phi} \int_{\Theta}^{\pi/2} \left((\min(r_{e+}, d))^3 - r_{e-}^3 \right) \sin\theta d\theta d\phi \quad (9)$$

where $r_{e\pm}$ are obtained from (5) under the constraints of (6) and $d \equiv R$.

Now, let us relate a, b, c and x_0 with system geometry. First, we set $x_0 \equiv D$, $b \equiv R_1$ and $c \equiv R_2$ (without loss of generality, we assume that $R_1 \geq R_2$). Our simulations have shown a strong dependence of model's accuracy on a. Based on simulation results and the fact that a should be expressed in terms of the networks radii, we have found that the overall accuracy increases significantly when we set[†] a equal to the quadrant of the ellipse[‡] with semi-axes the rest two semi-axes of the ellipsoid R_1 and R_2, that is, [21]:

$$a = R_1 E\left(\sqrt{1 - (R_2/R_1)^2}\right) \quad (10)$$

where $E(\cdot)$ is the complete elliptic integral of the second kind. For the sake of notation simplicity, the right side of (10) will be denoted by α_{R_1,R_2}.

As a result, the cdf of the distance between two uniformly distributed nodes within two circular-shaped networks when $D \geq \alpha_{R_1,R_2}$ is

$$F_d(d) \approx \frac{1}{\pi \alpha_{R_1,R_2} R_1 R_2} \int_0^{\Phi} \int_{\Theta}^{\pi/2} \left((\min(r_{e+}, d))^3 - r_{e-}^3 \right) \sin\theta d\theta d\phi \quad (11)$$

where $r_{e\pm}$ are given from (5) (under the constraints of (6)), and Φ, Θ from (8), by replacing a, b, c, and x_0 with α_{R_1,R_2}, R_1, R_2 and D, respectively.

Equation (11) is valid for $x_0 \geq a$, that is, when $D \geq \alpha_{R_1,R_2}$. In order to calculate $F_d(d)$ for $D < \alpha_{R_1,R_2}$, we have developed an empirical formula similar to (11). Our approach reduces, with simple

[†] The definition is among the simplest ones that has a clear physical meaning and provides adequate results in terms of solution accuracy.

[‡] This ellipse is also the projection of the ellipsoid on the $x = 0$ plane.

transformations, the size of the ellipsoid and the separation distance and calculates the distance cdf as before.

Let us consider an ellipsoid centered at D' with semi-axes $R'_{1,2} \equiv kR_{1,2}$ where k is a constant. In this case, it is also $\alpha_{R'_1,R'_2} = k\alpha_{R_1,R_2}$ due to (10). In the single disk scenario [2], simulations have shown that (11) gives adequate results for $R_{1,2} = R\alpha^2_{1,1}/4$ and $D = \alpha_{R,R}/2$ (R is the disk radius). Therefore, we expect that $R'_{1,2} = \left\{R\alpha^2_{1,1}/4, R_{1,2}\right\}$ at $D = \{0, \alpha_{R_1,R_2}\}$. As a result, the assumption of a linear relation between k and D gives

$$R'_{1,2} = \frac{1}{4}\left(\alpha^2_{1,1} + \frac{4-\alpha^2_{1,1}}{\alpha_{R_1,R_2}} D\right) R_{1,2} \tag{12}$$

Similarly, we expect that $D' = \{\alpha_{R_1,R_2}/2, \alpha_{R_1,R_2}\}$ at $D = \{0, \alpha_{R_1,R_2}\}$ which gives

$$D' = (\alpha_{R_1,R_2} + D)/2 \tag{13}$$

assuming a linear dependence of D' on D. However, in this case, simulations have indicated a more complex relation. Therefore, we extend (13) and write it as

$$D' = (\alpha_{R_1,R_2} + Dg(D))/2 \tag{14}$$

with $g(\alpha_{R_1,R_2}) = 1$. The $g(D) = D + 1 - \alpha_{R_1,R_2}$ is the simplest function that fulfils this constraint. Simulations have further shown that a value of D' that provides more accurate cdf values is obtained from the averaging of (13) and (14) . Thus, we set

$$D' \equiv \frac{1}{4}\left[2\alpha_{R_1,R_2} + D\left(D + 2 - \alpha_{R_1,R_2}\right)\right] \tag{15}$$

Working as before, we find that the intersection volume is

$$V' = \frac{4}{3}\int_0^{\pi}\int_0^{\pi/2}\left(\min\left(r'_{e+}, R\right)\right)^3 \sin\theta d\theta d\phi,\ \forall\phi \in [0,\pi],$$
$$\theta \in [0,\pi/2] : r'_{e+} \in \mathbf{R}^+ \tag{16}$$

where r'_{e+} is calculated from (5) under the constraints of (6) by replacing a, b, c, and x_0 with $\alpha_{R'_1,R'_2}$, R'_1, R'_2 and D'. In (16), we omit r^3_{e-} because $r_{e-} \notin \mathbf{R}^+$ in the original ellipsoid. Finally, the desired cdf is calculated (the volume of the ellipsoid is $4\pi\alpha_{R'_1,R'_2}R'_1R'_2\big/3$) from the expression

$$F_d(d) \approx \frac{1}{\pi\alpha_{R'_1,R'_2}R'_1R'_2}\int_0^{\pi}\int_0^{\pi/2}\left(\min\left(r'_{e+}, d\right)\right)^3 \sin\theta d\theta d\phi \tag{17}$$

4. MODEL VALIDATION

In this section, we validate the proposed model through simulations and comparisons with methods in the literature [1, 2, 6]. In the following examples, we set $R_1 = 1$ or $D = 1$; the rest of the distances are non-dimensional quantities normalized to R_1 or D, respectively.

First, we evaluate the model in representative scenarios that describe overlapping and non-overlapping networks, see Fig. 3. Table 1 gives the geometric parameters (R_1, R_2 and D) of each scenario.

Table 1. Networks geometric parameters ($R_1 = 1$).

Case	1(a)	1(b)	1(c)	1(d)	2(a)	2(b)	2(c)	2(d)
R_2	0.5	0.5	0.5	0.5	1	1	1	1
D	0.25	0.75	1.25	2	0	0.5	1.5	4

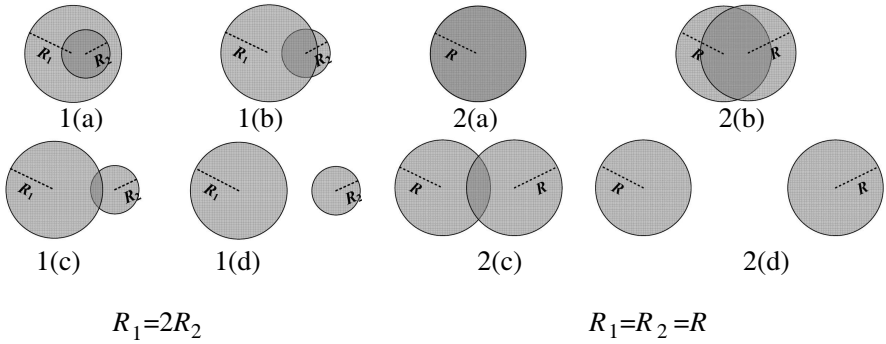

Figure 3. Illustration of networks coverage areas: Table's 1 scenarios.

Figure 4 illustrates the calculated and the empirical (simulation) distance cdf curves for the scenarios in Table 1. In the simulations, a single node was uniformly positioned inside each network using (1). In each scenario, we perform n independent simulation runs with different $r_{1,2}$ and $\phi_{1,2}$. The empirical cdf at distance d_i is

$$F_s\left(d_i\right) = \frac{1}{n}\sum_{j=1}^{n} u\left(d_i - d^j\right),\ i = 0, 1..N \tag{18}$$

with $d_i = \left(D + R_1 + R_2\right) i/N + \max\left(D - R_1 - R_2, 0\right)\left(1 - i/N\right)$, d^j the distance computed from (2) in the jth simulation run, $u\left(\cdot\right)$ the unit step function, $n = 10^7$ and $N = 100$.

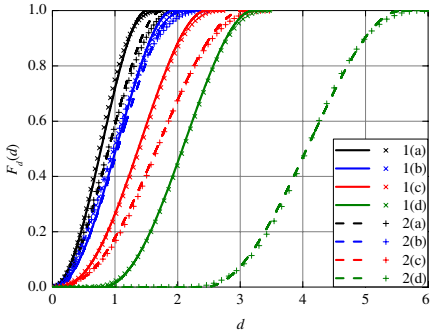

Figure 4. Distance cdf: calculated (curves) and simulation (symbols) results.

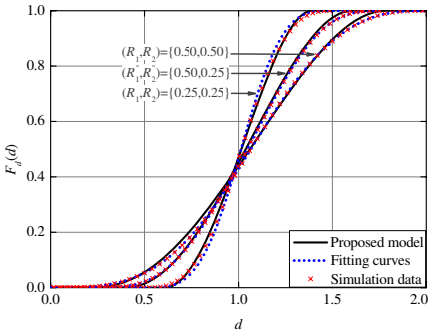

Figure 5. Distance distribution curves: calculated, fitting and simulation results.

Table 2. Mean absolute error between calculated and simulation results.

Case	1(a)	1(b)	1(c)	1(d)	2(a)	2(b)	2(c)	2(d)
$\bar{e} \times 10^2$	1.2963	1.8183	0.9104	0.6475	1.7372	2.4164	0.8441	0.8278

In the non-overlapping networks scenarios, calculated and simulation results are in close agreement. However, we notice that the accuracy of the model decreases slightly when the networks intersect.

In order to perform a quantitative analysis of the illustrated results, we compute the mean absolute error $\bar{e}$ between calculated and simulation results for the previous cases. This quantity is calculated from the expression

$$\bar{e} = \frac{1}{N} \sum_{i=0}^{N} |F_d(d_i) - F_s(d_i)| \tag{19}$$

where d_i is uniformly distributed in $[\max(D-R_1-R_2, 0), D+R_1+R_2]$. In our study, parameter N is 50. The results are presented in Table 2. Notice that $\bar{e}$ increases when the networks intersect, but it is always less than 2.5% of $\max F_d(d)$.

Figure 5 plots the distance cdf curves for the scenarios of non-overlapping networks with radii $(R_1, R_2) = \{(0.5, 0.5), (0.5, 0.25), (0.25, 0.25)\}$ and $D = 1$. The curves were obtained from (11), simulations and fitting formulas. The last were calculated by

Table 3. Mean absolute error between calculated, fitting and simulation results.

(R_1, R_2)	$\{0.5, 0.5\}$		$\{0.5, 0.25\}$		$\{0.25, 0.25\}$	
Case	*CS*	*CF*	*CS*	*CF*	*CS*	*CF*
$\bar{e} \times 10^3$	8.031	8.076	6.901	6.945	8.235	16.479

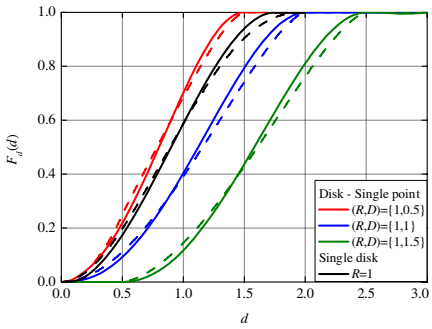

Figure 6. Distance cdf curves obtained from the proposed model (sold curves) and theory [1, 2] (dashed curves).

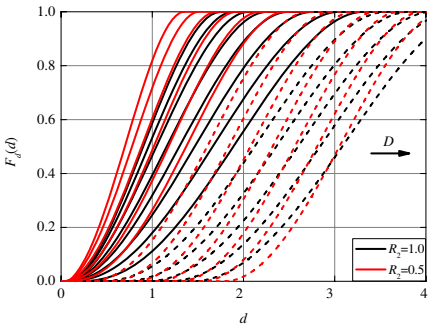

Figure 7. Impact of D on distance distribution function in overlapping (solid curves) and non-overlapping (dashed curves) networks.

integrating the corresponding empirical polynomial expressions[§] that describe distance density between pair of nodes in non-overlapping networks [6]. The three methods lead to similar results. Table 3 gives mean absolute error between calculated and simulation (*CS* col.) or fitting (*CF* col.) results. In all cases, the error is small.

We have already mentioned that the authors in [1] computed the cdf of the distance between a single point and a circle in closed-form; this problem has also been solved analytically for nodes uniformly distributed within the same circular disk [2]. In our model, these scenarios correspond to the cases $R_2 \to 0$ and $R_1 = R_2$, $D \to 0$, respectively. Here, we study certain representative examples of both scenarios. Fig. 6 shows that the cdf curves obtained from our model approximate the theoretical ones. In the first scenario, the differences are mainly due to the fact that the proposed model computes the

[§] Let set p_{R_i,R_j} where $R_i = i/10$ and $R_j = j/10$, $i, j = 1, 2..9 : \; i + j \leq 10$, the fitting polynomials (their coefficients are given in Tables 4-7 in [6]) that describe distance pdf for given $R_{1,2}$. The desired pdf is $p_{0.5,0.5}$ for $R_{1,2} = 0.5$. In the second and third scenarios, the pdfs are (see Section 4 in [6]) $(p_{0.2,0.5} + p_{0.3,0.5})/2$ and $(p_{0.2,0.2} + p_{0.3,0.3} + 2p_{0.2,0.3})/4$, respectively.

Table 4. Mean absolute error between calculated and theoretical [1, 2] results.

(R, D)	$\{1, 0.5\}$	$\{1, 1\}$	$\{1, 1.5\}$	$\{1, 0\}$
$\bar{e} \times 10^2$	1.7163	2.2856	2.4028	1.7216

distance cdf from the intersection volume of two solids instead of the intersection area of two plane objects (as in [1]). In other words, it solves a two-dimensional problem in the 3D space which increases the approximation error of (11) and (17). In the second scenario, networks fully overlap; thus, the approximation error of (17) reduces model's accuracy. Table 4 presents the mean absolute error between calculated and theoretical results for the previous cases. Comparison between the data in Tables 3 and 4, shows that $\bar{e}$ increases when the networks intersect, as it was expected.

In this section, representative examples demonstrated the efficacy of our approach. Comparisons with simulation and fitting results validated the accuracy of the model when the networks do not intersect. In this case, the mean absolute error between calculated and simulation results is less than 1%. When networks overlap, model's accuracy decreases slightly primarily due to the fact that (17) is an approximation of (11). In particular, error values up to 2.5% have been reported. However, even in this case, considering the simplicity of the model the results are adequate when we can not describe distance statistics in closed-form. At this point, recall that (10), (12) and (15) have been found empirically through simulations but achieve a good trade-off between complexity and accuracy. Obviously, more complex expressions would reduce the modeling error at the cost of higher complexity.

5. APPLICATIONS AND DISCUSSION

This section consists of two parts. Firstly, we investigate the impact of networks size and separation distance on the distance cdf. The results yield some interesting conclusions about the dependence of nodal distance on networks geometric parameters. In order to show the applicability of the method, we model distance-dependent path loss. A brief discussion of the relation between networks geometry, propagation characteristics and microwave signal attenuation completes the analysis.

5.1. Impact of Networks Geometry

Here, we explore the relation between distance cdf, separation distance and networks radii. In the following examples, we choose $R_1 = 1$ as reference distance.

Figure 7 plots distance cdf for D that ranges from 0 to 3 with steps equal to 0.25. The scenarios $R_2 = 1$ and $R_2 = 0.5$ are considered.

The cdf curves shift to the right with increasing D. In non-overlapping networks, any change in D shifts equally the cdf curve along the d-axis; the shift is smaller when networks intersect. Apart from this, in the second case, curves are always minimized at $d = 0$. Comparing the scenarios with different radius, we see that the cdf curves shift to the right when $R_2 = 1$; the slope of the cdf curves varies also.

Next, we investigate the impact of networks radii on distance cdf. The separation distance is 0.5 and 2 (first and second scenarios, respectively). In the first (second) scenario, R_2 varies from 0 to 2 (0 to 4) with step 0.2 (0.4). In the first case, the networks intersect because $D < R_1$; in the second one, they overlap only when $R_2 > 1$. The distance cdf curves are plotted in Figs. 8 and 9, respectively.

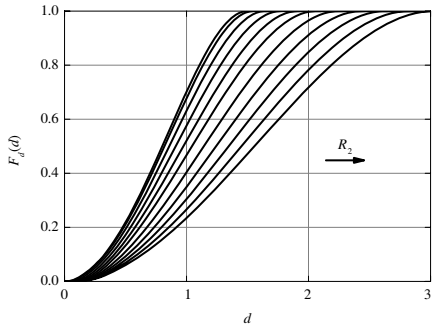

Figure 8. Impact of networks radii on $F_d(d)$; R_2 varies from 0 to 2 with step 0.2.

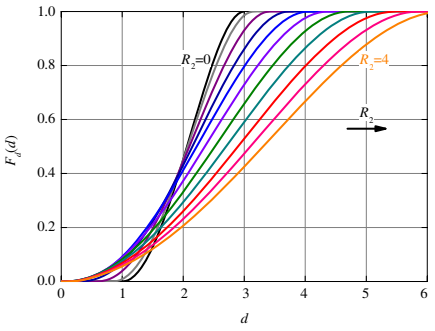

Figure 9. Impact of networks radii on $F_d(d)$; R_2 varies from 0 to 4 with step 0.4.

Figure 8 shows that the cdf curves shift to the right with increasing R_2. The shift increases with R_2 up to a point beyond which it remains constant. On the other hand, the slope of the curves decreases with R_2. In Fig. 9, we observe a similar behavior for overlapping networks. However, if the networks do not overlap, the cdf curves intersect at $d \approx D$ and the minimum (maximum) d at which the cdf is one (zero) increases (decreases) with R_2.

5.2. An Application in Radio Wave Propagation

The prediction of microwave attenuation [22–33] is important in the analysis of wireless systems. Signal propagation is strongly affected by the dissipation of the power radiated by the transmitter that is related to the distance between the communicating nodes. The distance-dependent path loss at a distance d is usually expressed in natural units as

$$L = L_0 \left(d_0/d\right)^n \tag{20}$$

where L_0 is the path loss at a reference distance d_0 and n is the path loss exponent [34–36]. For notational simplicity, we set $d_0 \equiv D$ and $L_0 = 0$ dB (similar assumptions are common in the literature, e.g., [5, 6]) and (20) becomes

$$L = \left(D/d\right)^n \tag{21}$$

In this context, $F_L\left(L\right)$ is obtained from $F_d\left(d\right)$. For this reason, we determine the set of the d-axis such that $\left(D/d\right)^n \leq L$ (due to (21)). Obviously, it is

$$F_L\left(L\right) = \text{Prob}\left[d \geq DL^{-1/n}\right] = 1 - F_d\left(DL^{-1/n}\right) \tag{22}$$

where $\text{Prob}\left[d \geq DL^{-1/n}\right]$ is the probability that nodal distance d is greater than $DL^{-1/n}$.

As a sample application, we consider the scenarios with networks radii $\left(R_1, R_2\right) = \left\{\left(D/4, D/4\right), \left(D/2, D/4\right), \left(D/2, D/2\right)\right\}$ (cases (a)–(c), respectively). In the illustrated examples, n takes the values 2, 4.2 and 7.7 that correspond to free-space, urban and dual carriage

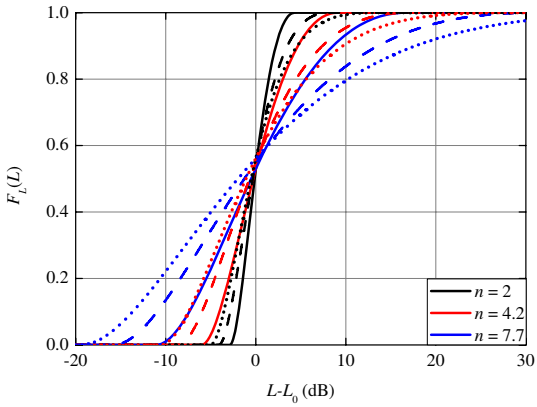

Figure 10. Distance dependent path loss cdf curves; case (a): solid curves, case (b): dashed curves, case (c): dotted curves.

highway propagation, respectively [22]. Fig. 10 illustrates the distance-dependent path loss cdf curves as a function of the difference $L - L_0$ (in dB). Clearly, path loss cdf depends on both path loss exponent and system geometry. The curves shift to the right with increasing n, which means that the transmission range decreases with n, and show a stronger dependence on n as the networks coverage areas approach to each other. Similar conclusions were drawn in [6].

6. CONCLUSION

We presented a geometrical-based model for the calculation of the cumulative distribution function of the distance between uniformly distributed nodes in circular-shaped networks. The derived results are in close agreement with data obtained from fitting methods in the literature and simulations. Comparisons with theory showed that the method adequately describes the nodal distance cdf in single networks also. The study of the impact of networks geometric parameters on distance statistics clarified basic differences between overlapping and non-overlapping networks. In a sample application, we modeled distance-dependent path loss and discussed the relation between system geometry, path loss exponent and signal absorption. The method computes distance cdf without complicated calculations and provides adequate accuracy. It is a useful tool for system-level simulations of wireless networks with applications in mobile networking.

REFERENCES

1. Adelantado, F., J. Pérez-Romero, and O. Sallent, "Nonuniform traffic distribution model in reverse link of multirate/multiservice WCDMA-based systems," *IEEE Transactions on Vehicular Technology*, Vol. 56, 2902–2914, 2007.
2. Sinanović, S., N. Serafimovski, H. Haas, and G. Auer, "Maximizing the system spectral efficiency in a decentralised 2-link wireless network," *EURASIP Journal on Wireless Communications and Networking*, 2008, doi:10.1155/2008/867959.
3. Kaltenberger, F., M. Kountouris, D. Gesbert, and R. Knopp, "On the trade-off between feedback and capacity in measured MU-MIMO channels," *IEEE Transactions on Wireless Communications*, Vol. 8, 4866–4875, 2009.
4. Ali, A., L. A. Latiff, and N. Fisal, "Simulation-based real-time routing protocol with load distribution in wireless sensor

networks," *Wireless Communications and Mobile Computing*, Vol. 10, 1002–1016, 2010.

5. Kumar, D., R. Venkatesh, A. Kumar, and E. Altman, "Capacity optimizing hop distance in a mobile ad hoc network with power control," *4th International Symposium on Modeling and Optimization in Mobile, Ad Hoc and Wireless Networks (WiOPT 2006)*, Boston, USA, 2006, doi:10.1109/WIOPT.2206.1666452.
6. Baltzis, K. B., "Empirical description of node-to-node distance density in non-overlapping wireless networks," *Journal of Microwaves, Optoelectronics and Electromagnetic Applications*, Vol. 9, No. 1, 57–68, 2010.
7. De Carlo, D. and S. Tringàli, "Automatic design of circular SIW resonators by a hybrid approach based on polynomial fitting and SVRMS," *Journal of Electromagnetic Waves and Applications*, Vol. 24, No. 5–6, 735–774, 2010.
8. Dessouky, M. I., H. A. Sharshar, and Y. A. Albagory, "Geometrical analysis of high altitude platforms cellular footprint," *Progress In Electromagnetics Research*, Vol. 67, 263–274, 2007.
9. Chen, Y., Z. Zhang, L. Hu, and P. Rapajic, "Geometry-based statistical model for radio propagation in rectangular office buildings," *Progress In Electromagnetics Research B*, Vol. 17, 187–212, 2009.
10. Baltzis, K. B. and J. N. Sahalos, "A simple 3-D geometric channel model for macrocell mobile communications," *Wireless Personal Communications*, Vol. 51, 329–347, 2009.
11. Baltzis, K. B. and J. N. Sahalos, "On the statistical description of the AoA of the uplink interfering signals in a cellular communication system," *European Transactions on Telecommunications*, Vol. 21, 187–194, 2010.
12. Chen, Y., Z. Zhang, and T. Qin, "Geometrically based channel model for indoor radio propagation with directional antennas," *Progress In Electromagnetics Research B*, Vol. 20, 109–124, 2010.
13. Nawaz, S. J., B. H. Qureshi, and N. M. Khan, "A generalized 3-D scattering model for a macrocell environment with a directional antenna at the BS," *IEEE Transactions on Vehicular Technology*, Vol. 59, 3193–3204, 2010.
14. Wang, A.-Q., L.-X. Guo, and C. Chai, "Numerical simulations of electromagnetic scattering from 2D rough surface: Geometric modeling by nurbs surface," *Journal of Electromagnetic Waves and Applications*, Vol. 24, No. 10, 1315–1328, 2010.
15. Alsehaili, M., S. Noghanian, A.-R. Sebak, and D. A. Buchanan,

"Angle and time of arrival statistics of a three dimensional geometrical scattering channel model for indoor and outdoor propagation environments," *Progress In Electromagnetics Research*, Vol. 109, 191–209, 2010.

16. Pirinen, P., "Outage analysis of ultra-wideband system in lognormal multipath fading and square-shaped cellular configurations," *EURASIP Journal on Wireless Communications and Networking*, 2006, doi:10.1155/WCN/2006/19460.
17. Haenggi, M., "A geometric interpretation of fading in wireless networks: Theory and applications," *IEEE Transactions on Information Theory*, Vol. 54, 5500–5510, 2008.
18. Kyatkin, A. B. and G. S. Chirikjian, "Computation of robot configuration and workspaces via the Fourier transform on the discrete-motion group," *The International Journal of Robotics Research*, Vol. 18, 601–615, 1999.
19. Tu, S.-J. and E. Fischbach, "Random distance distribution for spherical objects: General theory and applications to physics," *Journal of Physics A: Mathematical and General*, Vol. 35, 6557–6570, 2002.
20. Akhriev, A., "Object tracking via uncertainty minimization," *Lecture Notes in Computer Science: Advances in Visual Computing*, Vol. 4842, 592–601, Springer, Berlin, 2007.
21. Weisstein, E. W., *CRC Concise Encyclopedia of Mathematics*, 2nd edition, Chapman & Hall/CRC, Boca Raton, 2003.
22. Agbinya, J. I., "Design considerations of MoHotS and wireless chain networks," *Wireless Personal Communications*, Vol. 40, 91–106, 2007.
23. Roozbahani, M. G., E. Jedari, and A. A. Shishegar, "A new link-level simulation procedure of wideband MIMO radio channel for performance evaluation of indoor WLANs," *Progress In Electromagnetics Research*, Vol. 83, 13–24, 2008.
24. Kara, A. and E. Yazgan, "Modelling of shadowing loss due to huge non-polygonal structures in urban radio propagation," *Progress In Electromagnetics Research B*, Vol. 6, 123–134, 2008.
25. Phaiboon, S. and P. Phokharatkul, "Path loss prediction for low-rise buildings with image classification on 2-D aerial photographs," *Progress In Electromagnetics Research*, Vol. 95, 135–152, 2009.
26. Gennarelli, G. and G. Riccio, "A uapo-based model for propagation prediction in microcellular environments," *Progress In Electromagnetics Research B*, Vol. 17, 101–116, 2009.
27. Meng, Y. S., Y. H. Lee, and B. C. Ng, "Study of propagation loss

prediction in forest environment," *Progress In Electromagnetics Research B*, Vol. 17, 117–133, 2009.

28. Howitt, I. L. and M. S. Khan, "A mode based approach for characterizing RF propagation in conduits," *Progress In Electromagnetics Research B*, Vol. 20, 49–64, 2010.
29. Jung, J.-W., D. S. Kim, D. G. Cho, and Y.-S. Kim, "Required guardband for coexisting LTE/FDD systems obtained by accurate analysis of adjacent channel interference," *Journal of Electromagnetic Waves and Applications*, Vol. 24, No. 14–15, 2095–2106, 2010.
30. Baltzis, K. B., "On the effect of channel impairments on VANETs performance," *Radioengineering*, Vol. 19, 689–694, 2010.
31. Baltzis, K. B., "Analytical and closed-form expressions for the distribution of path loss in hexagonal cellular networks," *Wireless Personal Communications*, 2010, doi:10.1007/s11277-010-9962-2.
32. Gao, Y.-Y., X.-X. Yang, C. Jiang, and J.-Y. Zhou, "A circularly polarized rectenna with low profile for wireless power transmission," *Progress In Electromagnetics Research Letters*, Vol. 13, 41–49, 2010.
33. Pu, S., J.-H. Wang, and Z. Zhang, "Estimation for small-scale fading characteristics of RF wireless link under railway communication environment using integrative modeling technique," *Progress In Electromagnetics Research*, Vol. 106, 395–417, 2010.
34. Das, S., A. Maitra, and A. K. Shukla, "Rain attenuation modeling in the 10–100 GHz frequency using drop size distributions for different climatic zones in tropical India," *Progress In Electromagnetics Research B*, Vol. 25, 211–224, 2010.
35. Spiliotopoulos, C. G. and A. G. Kanatas, "Channel measurements and modelling in a military cargo airplane," *Progress In Electromagnetics Research B*, Vol. 26, 69–100, 2010.
36. Masa-Campos, J. L., J. M. Lalueza-Mayordomo, and B. Taha-Ahmed, "RF propagation in indoor environment at WIMAX band of 3.5 GHz," *Journal of Electromagnetic Waves and Applications*, Vol. 24, No. 17–18, 2495–2508, 2010.